**Supplementary Table S1. The differentially expressed genes (DEGs) in sh*Phf23* pre-B cells compared to those with sh*Ren*.**

**Supplementary Table S2. Unique proteins Co-IP with FLAG-PHF23, identified with LC/MS.**

| Protein name | #Unique peptides | #Total peptides | Coverage | Score |
|---|---|---|---|---|
| PHF23 | 11 | 11 | 23 | 988 |
| SIN3A | 25 | 26 | 28 | 829 |
| SIN3B | 9 | 10 | 12 | 109 |
| SAP130 | 6 | 6 | 10 | 189 |
| FAM60A | 6 | 6 | 35 | 162 |
| HDAC1 | 4 | 4 | 12 | 160 |
| ARID4B | 4 | 4 | 4 | 132 |
| SUDS3 | 3 | 3 | 10 | 76 |
| SAP30L | 3 | 3 | 23 | 76 |
| BRMS1L | 3 | 3 | 9 | 43 |
| RBBP7 | 2 | 5 | 11 | 130 |
| RBBP4 | 1 | 4 | 8 | 145 |
| SAP30 | 1 | 1 | 5 | 66 |
| HDAC2 | 1 | 1 | 2 | 59 |

**Supplementary Table S3. The DEGs in sh*Phf23* lymphoma/leukemia cells compared to those with sh*Ren*.**

**Supplementary Table S4. The DEGs in sh*Phf23* lymphoma/leukemia cells treated with chidamide or entinostat, comparing to those treated with DMSO.**

**Supplementary Table S5. Sequences of shRNAs used in this study.**

| Gene Name | shRNA sequences |
|---|---|
| sh*Phf23.338* | TGCTGTTGACAGTGAGCGCACCATTGAGGATTTTAA CAAATAGTGAAGCCACAGATGTATTTGTTAAAATCC TCAATGGTTTGCCTACTGCCTCGGA |
| sh*Phf23.877* | TGCTGTTGACAGTGAGCGCAAAGCGGTCTCGAATCA AGAATAGTGAAGCCACAGATGTATTCTTGATTCGAG ACCGCTTTTTGCCTACTGCCTCGGA |
| sh*Phf23.971* | TGCTGTTGACAGTGAGCGCCCCAGTGATACAGACTC TGAATAGTGAAGCCACAGATGTATTCAGAGTCTGTA TCACTGGGATGCCTACTGCCTCGGA |
| sh*Sin3a.918* | TGCTGTTGACAGTGAGCGCTGCCATCAACTATGTTAA TAATAGTGAAGCCACAGATGTATTATTAACATAGTTG ATGGCATTGCCTACTGCCTCGGA |
| sh*Sin3a.2346* | TGCTGTTGACAGTGAGCGCTGAAGACAAACAGATACT AGATAGTGAAGCCACAGATGTATCTAGTATCTGTTTG TCTTCATTGCCTACTGCCTCGGA |
| sh*Sin3b.513* | TGCTGTTGACAGTGAGCGCCAGCTATGTGAACAAGAT CAATAGTGAAGCCACAGATGTATTGATCTTGTTCACA TAGCTGATGCCTACTGCCTCGGA |
| sh*Sin3b.573* | TGCTGTTGACAGTGAGCGCCCTGGAGATCCTACACAC CTATAGTGAAGCCACAGATGTATAGGTGTGTAGGATC TCCAGGATGCCTACTGCCTCGGA |
| sh*Hdac1.256* | TGCTGTTGACAGTGAGCGACCCAGATAATATGTCTGA ATATAGTGAAGCCACAGATGTATATTCAGACATATTA TCTGGGCTGCCTACTGCCTCGGA |
| sh*Hdac1.1529* | TGCTGTTGACAGTGAGCGCCCTCTGTGTATTTATATAA AATAGTGAAGCCACAGATGTATTTTATATAAATACAC AGAGGATGCCTACTGCCTCGGA |

**Supplementary Table S6. qPCR primers**

| Gene Name | Primer sequences |
|---|---|
| RT-*Phf23*-F | CTTGGCCTATGCTGGTTACA |
| RT-*Phf23*-R | CACTGTCTGCTGCACTCTC |
| RT-*Sin3a*-F | AGTTTCAGAGGCTCAAGGTG |
| RT-*Sin3a*-R | GAGGCTGACTACCGAACTG |
| RT-*Sin3b*-F | CCGCTTGGATACCGTATAGAC |
| RT-*Sin3b*-R | CATGGCTATGGGAGTTGTCC |
| RT-*Hdac1*-F | GCTCAACTATGGTCTCTACCG |
| RT-*Hdac1*-R | CACTGTGGTACTTGGTCATCTC |

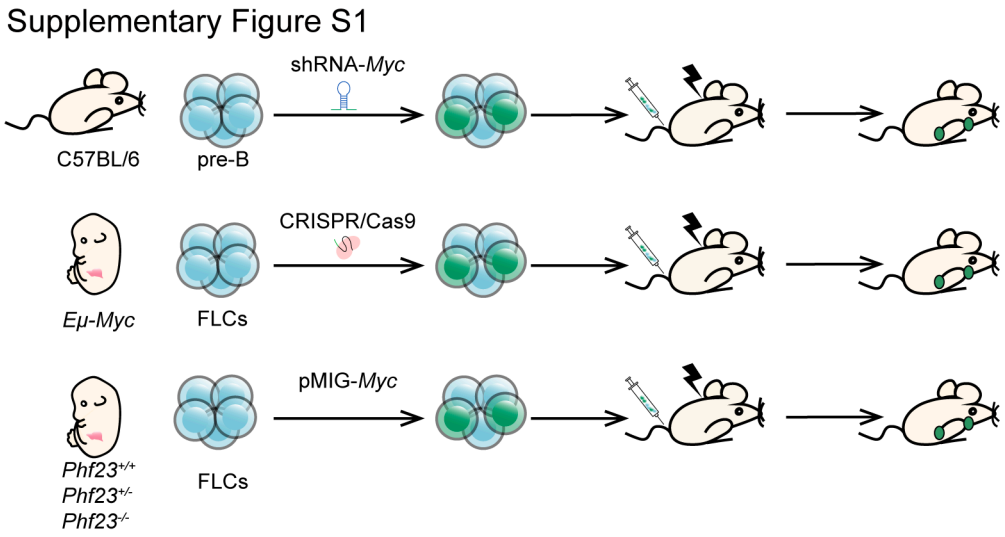


**Figure S1 | Schematic diagram showing the strategies for the *in vivo* functional studies of *Phf23* in tumorigenesis.**

Top, Schematic diagram showing the procedure of transplantation of recipient mice with pre-B infected with *Myc*-linked shRNAs. Middle, Schematic diagram showing the procedure of transplantation of recipient mice with *Eμ-Myc* FLCs infected with CRISPR/Cas9 system. Bottom, Schematic diagram showing the procedure of transplantation of recipient mice with $Phf23^{+/+}$, $Phf23^{+/-}$, $Phf23^{-/-}$ FLCs infected with GFP linked *Myc* cDNA.

Supplementary Figure S2

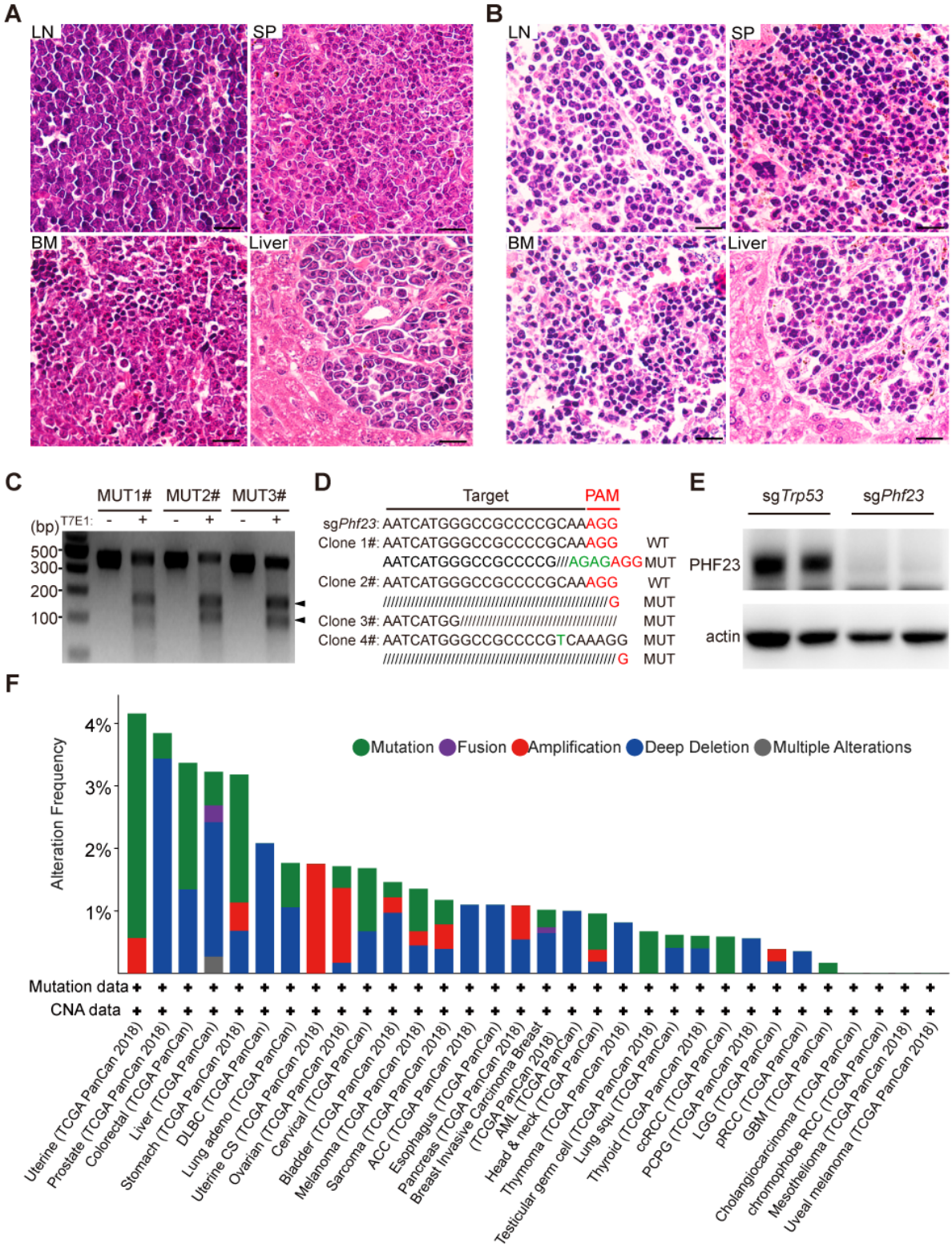


**Figure S2 | Characterizations of *Phf23* deficient tumors and *PHF23* mutations in human cancer.**

A, Representative pictures showing H/E staining of lymph node (LN), spleen (SP), bone marrow (BM) and liver tissues of recipient mice with sh*Phf23* pre-B cells in Fig. 1C. Scale bar, 20$\mu$m. B, Representative pictures showing H/E staining of LN, SP, BM and liver tissues of recipient mice with sg*Phf23* FLCs in Fig. 1H. Scale bar, 20$\mu$m. C, Mutations on *Phf23* in

sg*Phf23* lymphoma/leukemia cells from recipient mice in Fig. 1H, measured by T7E1 assay. D, Sanger sequencing analysis of genomic *Phf23* DNA sequences in sg*Phf23* tumor cell clones. E, Representative Western blotting picture showing the protein levels of PHF23 in sg*Phf23* lymphoma/leukemia cells. F, Histogram showing the alterations of *PHF23* in TCGA PanCancer, analyzed from cBioPortal.

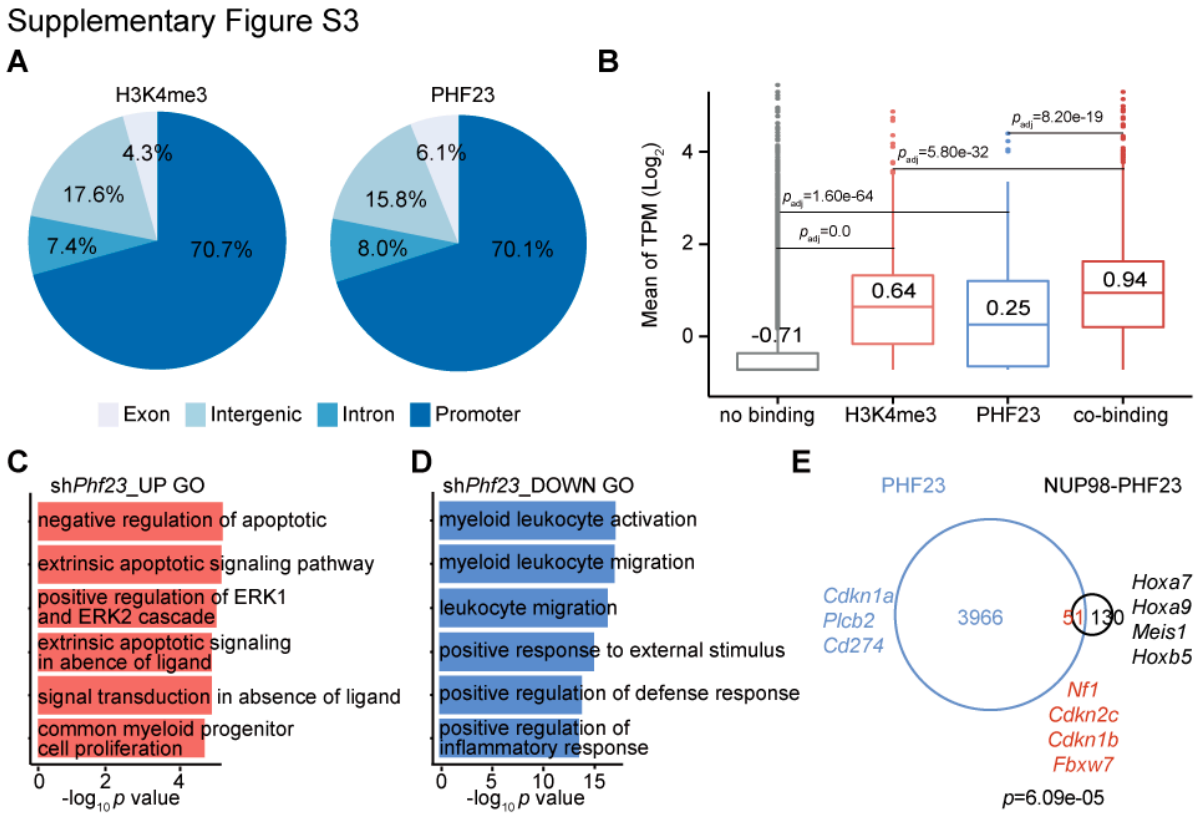


**Figure S3 | PHF23 co-located with H3K4me3 and regulated gene expression.**
A, Genome-wide distribution of H3K4me3 (left) and PHF23 (right) bound peaks in Ba/F3 cells, measured by ChIP-seq analysis. B, Mean $\log_2$ TPM of genes with no binding (without H3K4me3 and PHF23 binding), H3K4me3 only, PHF23 only and co-binding (both H3K4me3 and PHF23 binding) in pre-B cells. $p_{adj}$,Wilcoxon signed-rank test. C, The Gene Ontology (GO) enrichment plot of the upregulated genes in sh*Phf23* pre-B cells compared to sh*Ren* pre-B cells. D, The GO enrichment plot of the downregulated genes in sh*Phf23* pre-B cells compared to sh*Ren* pre-B cells. E, Venn diagram showing overlapping of PHF23 and NUP98-PHF23 bound genes; *p*, Fisher's exact test.

Supplementary Figure S4

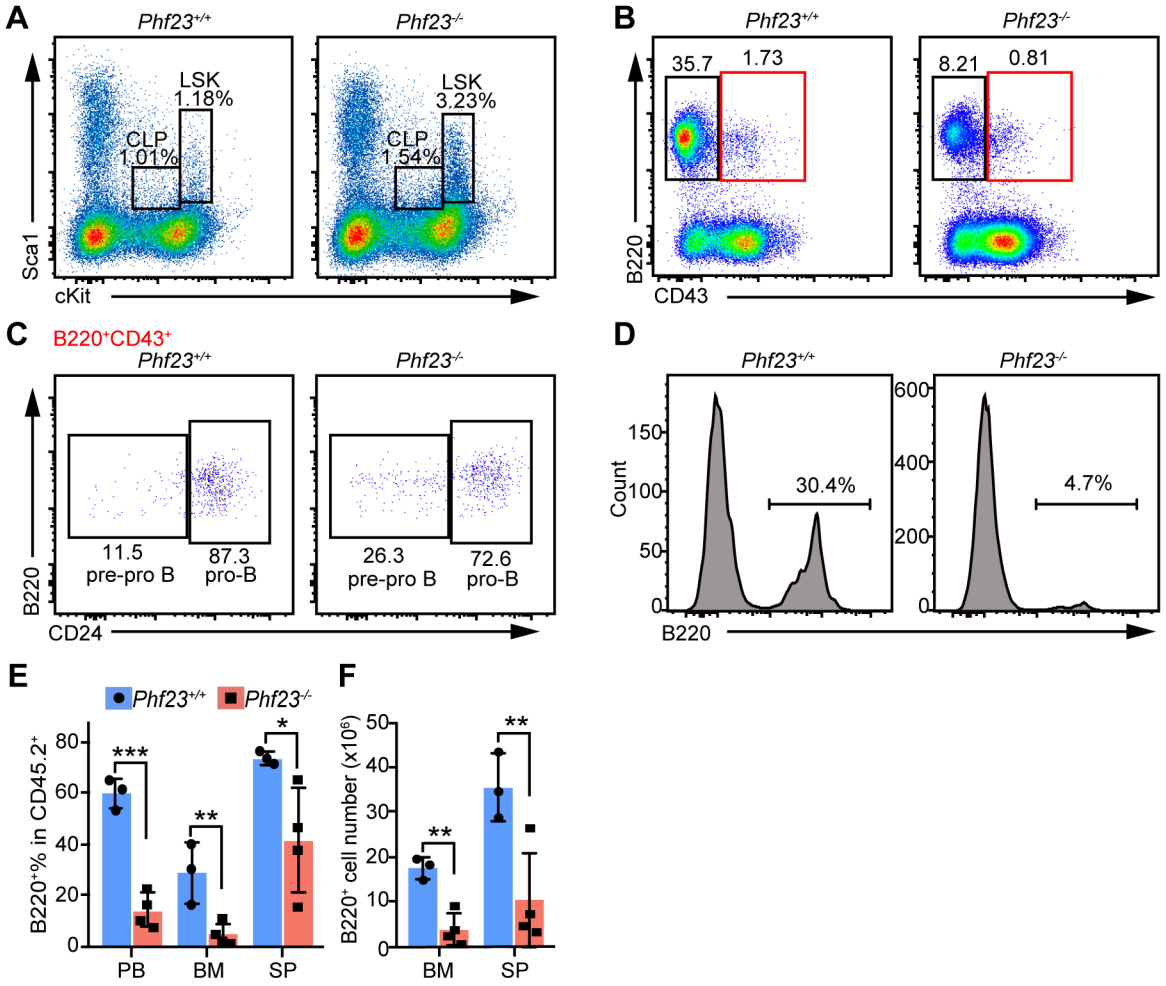


**Figure S4 | *Phf23* loss impaired the B cell differentiation in mice.**
A, Representative flow plots showing percentages of donor-type LSK and CLP populations in Lin$^-$ BM cells of recipient mice 4 months after BMT, from the experiment shown in Fig. 3G. B, Representative flow plots showing percentages of B220$^+$CD43$^+$ and B220$^+$CD43$^-$ populations gated in donor-type BM cells. C, Representative flow plots showing percentages of CD24$^-$ (pre-pro B), CD24$^+$ (pro-B) gated in B220$^+$CD43$^+$ cells. D, Representative flow plots showing percentages of donor-type B220$^+$ cell in BM of recipient mice. E, Percentages of donor-type B220$^+$ population in peripheral blood (PB), bone marrow (BM) and spleen (SP) of recipient mice. F, Numbers of donor-type B220$^+$ cells in BM and spleen of recipient mice. E-F, *$p$<0.05, **$p$<0.01, ***$p$<0.001 ($t$-test).

Supplementary Figure S5

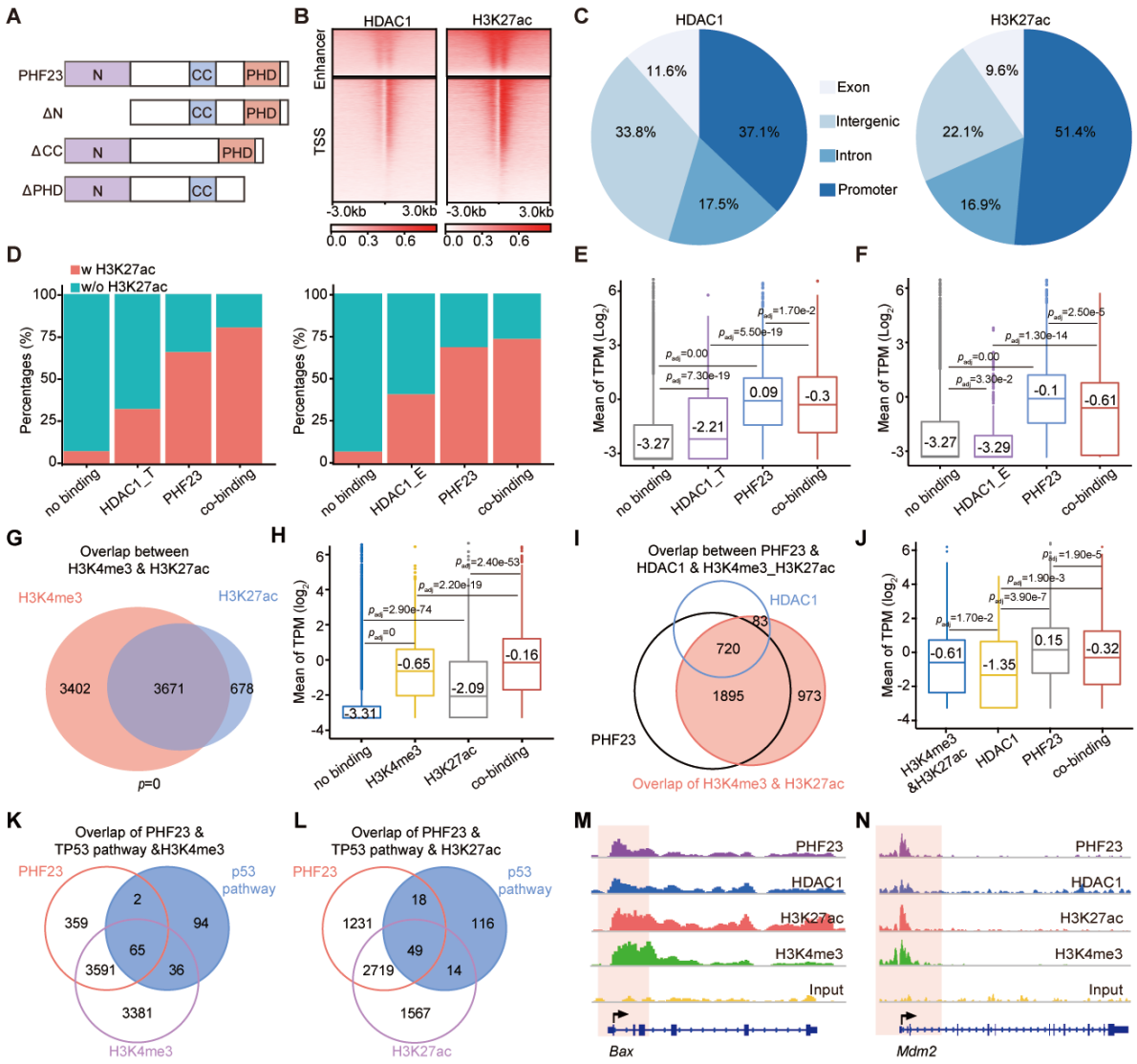


**Figure S5 | PHF23 negatively regulated the SIN3-HDAC complex.**

A, Schematic diagram of full length and truncated PHF23. ΔN, N terminus truncated; ΔCC, coiled-coil domain truncated; and ΔPHD, PHD domain truncated. B, heatmaps showing HDAC1 and H3K27ac bound peaks in enhancer (top) and TSS (bottom) regions, analyzed by ChIP-seq. C, Genome distribution of HDAC1 peaks (left) and H3K27ac peaks (right). D, Left, stacked bar graphs showing percentages of genes with or without (w/o) H3K27ac binding in no binding (without HDAC1 TSS and PHF23 binding), HDAC1_T (only HDAC1 TSS binding), PHF23 (only PHF23 binding) or co-binding (both have HDAC1 TSS and PHF23 binding) genes. Right, stacked bar graphs showing percentages of genes with or without H3K27ac binding in no binding (without HDAC1 enhancer and PHF23 binding), HDAC1_E (only HDAC1 enhancer binding), PHF23 (only PHF23 binding) or co-binding (both have HDAC1 enhancer and PHF23 binding) genes. E, Mean of $\log_2$ TPM of genes with no binding (without HDAC1 TSS and PHF23 binding), HDAC1_T (only HDAC1 TSS binding), PHF23 (only PHF23 binding) or co-binding (both have HDAC1 TSS and PHF23 binding) in pre-B cells. $p_{adj}$, Wilcoxon signed-rank test. F, Mean of $\log_2$ TPM of genes with no binding (without

HDAC1 enhancer and PHF23 binding), HDAC1_E (only HDAC1 enhancer binding), PHF23 (only PHF23 binding) or co-binding (both have HDAC1 enhancer and PHF23 binding) in pre-B cells. $p_{adj}$, Wilcoxon signed-rank test. G, Venn diagram showing overlapping of H3K4me3 and H3K27ac bound genes; $p$ by Fisher's exact test. H, Mean $\log_2$ TPM in no binding (without H3K4me3 and H3K27ac binding), H3K4me3 (only H3K4me3 binding), H3K27ac (only H3K27ac binding), co-binding (both have H3K4me3 and H3K27ac binding) in pre-B cells. $p_{adj}$ by Wilcoxon signed-rank test. I, Venn diagram showing overlapping of PHF23, HDAC1 and overlapping of H3K4me3 and H3K27ac bound genes. J, Mean $\log_2$ TPM in H3K4me3_H3K27ac (H3K4me3 and H3K27ac overlapping genes), HDAC1 (HDAC1 and H3K4me3_H3K27ac overlapping genes without PHF23 binding), PHF23 (PHF23 and H3K4me3_H3K27ac overlapping genes without HDAC1 binding), co-binding (PHF23, HDAC1 and H3K4me3_H3K27ac overlapping genes) in pre-B cells. $p_{adj}$ by Wilcoxon signed-rank test. K, Venn diagram showing overlapping of PHF23, H3K4me3 bound genes and p53 pathway genes. L, Venn diagram showing overlapping of PHF23, H3K27ac bound genes and p53 pathway genes. M, IGV plots showing PHF23, HDAC1, H3K27ac and H3K4me3 binding density on *Bax*. N, IGV plots showing PHF23, HDAC1, H3K27ac and H3K4me3 binding density on *Mdm2*.

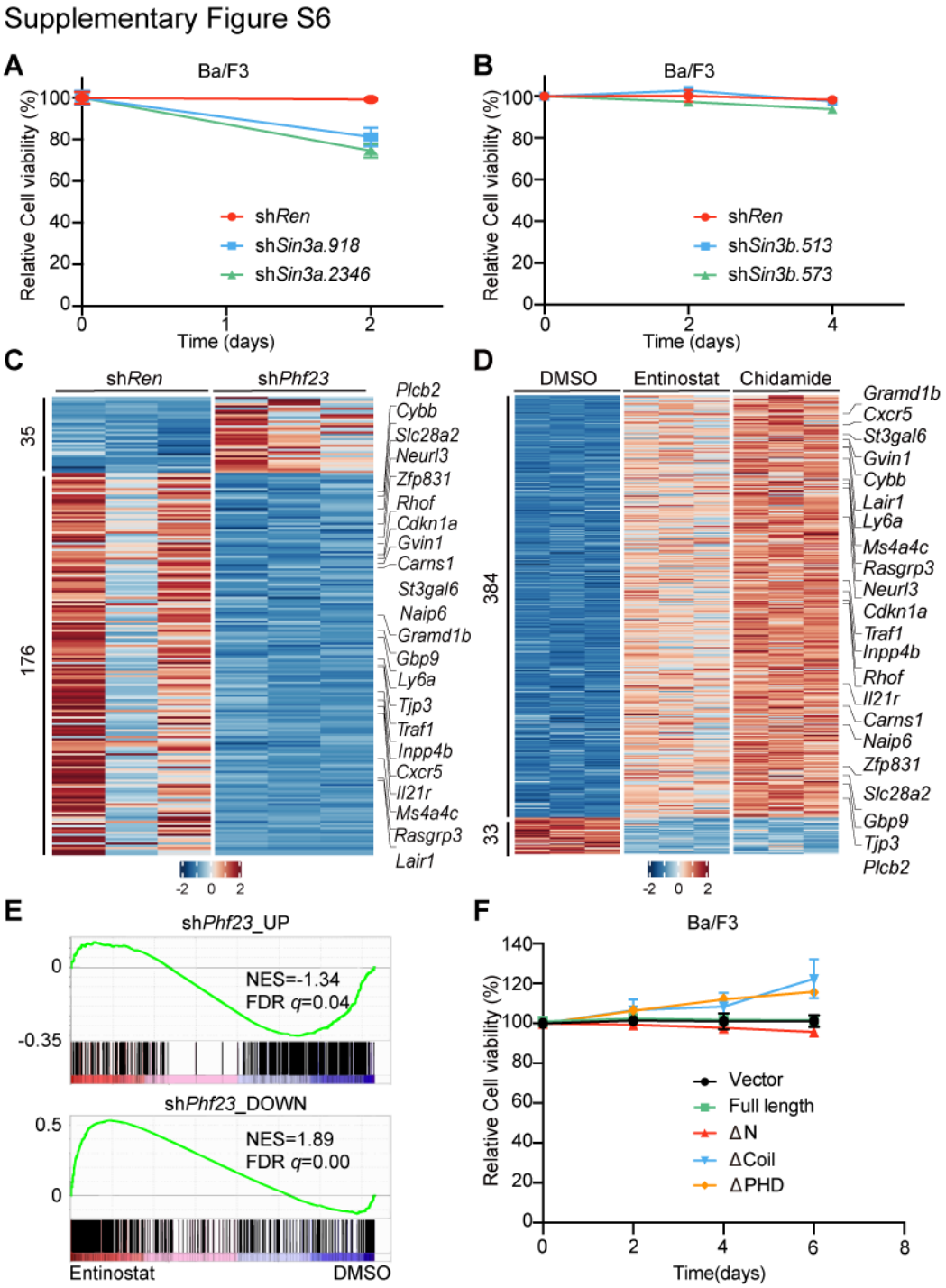


**Figure S6 | The role of the PSH complex in tumor maintenance.**
A, Relative cell viabilities of Ba/F3 cells with sh*Sin3a*. n=3. B, Relative cell viabilities of Ba/F3 cells with sh*Sin3b*. n=3. C, Heatmap showing the DEGs ($p_{adj}$<0.05, $\log_2$ Fold change>1 or < -1) in sh*Phf23* lymphoma/leukemia cells compared to those with sh*Ren*, measured by RNA-seq analysis. D, Heatmap showing the DEGs ($p_{adj}$<0.05, $\log_2$ Fold change>1 or <-1) in entinostat and chidamide treated sh*Phf23* lymphoma/leukemia cells compared to those treated with DMSO, measured by RNA-seq analysis. E, Top, GSEA showing the negative enrichment of the sh*Phf23* upregulated gene set in entinostat treated sh*Phf23* lymphoma/leukemia cells, comparing to DMSO treated cells (NES=-1.34; FDR $q$=0.04). Bottom, GSEA showing the positive enrichment of the sh*Phf23* downregulated gene set in entinostat treated sh*Phf23*

lymphoma/leukemia cells, comparing to DMSO treated cells (NES=1.89; FDR *q*=0.00). F, Relative cell viabilities of Ba/F3 cells transduced with full-length or truncated *Phf23*. n=3.